Mutation in human *CLPX* elevates levels of δ-aminolevulinate synthase and protoporphyrin IX to promote erythropoietic protoporphyria

Yvette Y. Yien[a,1], Sarah Ducamp[b,c,d,1,2], Lisa N. van der Vorm[a,3,4], Julia R. Kardon[e,f,3], Hana Manceau[b,c,d], Caroline Kannengiesser[b,d,g], Hector A. Bergonia[h], Martin D. Kafina[a], Zoubida Karim[b,c,d], Laurent Gouya[b,c,d], Tania A. Baker[e,f,5], Hervé Puy[b,c,d,5], John D. Phillips[h,5], Gaël Nicolas[b,c,d,6], and Barry H. Paw[a,i,j,5,6]

[a]Division of Hematology, Brigham & Women's Hospital, Harvard Medical School, Boston, MA 02115; [b]INSERM U1149, CNRS ERL 8252, Centre de Recherche sur l'inflammation, Université Paris Diderot, Site Bichat, Sorbonne Paris Cité, 75018 Paris, France; [c]Assistance Publique-Hôpitaux de Paris, Centre Français des Porphyries, Hôpital Louis Mourier, 92701 Colombes Cedex, France; [d]Laboratory of Excellence, GR-Ex, 75015 Paris, France; [e]Department of Biology, Massachusetts Institute of Technology, Cambridge, MA 02139; [f]Howard Hughes Medical Institute, Massachusetts Institute of Technology, Cambridge, MA 02139; [g]Département de Génétique, Assistance Publique-Hôpitaux de Paris, HUPNVS, Hôpital Bichat, 75877 Paris Cedex, France; [h]Division of Hematology, University of Utah School of Medicine, Salt Lake City, UT 84112; [i]Division of Hematology-Oncology, Boston Children's Hospital, Harvard Medical School, Boston, MA 02115; and [j]Department of Pediatric Oncology, Dana-Farber Cancer Institute, Harvard Medical School, Boston, MA 02115

Loss-of-function mutations in genes for heme biosynthetic enzymes can give rise to congenital porphyrias, eight forms of which have been described. The genetic penetrance of the porphyrias is clinically variable, underscoring the role of additional causative, contributing, and modifier genes. We previously discovered that the mitochondrial AAA+ unfoldase ClpX promotes heme biosynthesis by activation of δ-aminolevulinate synthase (ALAS), which catalyzes the first step of heme synthesis. CLPX has also been reported to mediate heme-induced turnover of ALAS. Here we report a dominant mutation in the ATPase active site of human CLPX, p.Gly298Asp, that results in pathological accumulation of the heme biosynthesis intermediate protoporphyrin IX (PPIX). Amassing of PPIX in erythroid cells promotes erythropoietic protoporphyria (EPP) in the affected family. The mutation in *CLPX* inactivates its ATPase activity, resulting in coassembly of mutant and WT protomers to form an enzyme with reduced activity. The presence of low-activity CLPX increases the posttranslational stability of ALAS, causing increased ALAS protein and ALA levels, leading to abnormal accumulation of PPIX. Our results thus identify an additional molecular mechanism underlying the development of EPP and further our understanding of the multiple mechanisms by which CLPX controls heme metabolism.

heme biosynthesis | porphyria | ALAS | protein unfoldases | AAA+ ATPase

Porphyrias result from disorders of heme synthesis and are associated with mutations in numerous heme synthetic enzymes (1). The genetic penetrance of porphyria-causing alleles is variable, however (1–3), often due to the presence of diverse environmental factors and the existence of modifier genes. In addition, some patients with porphyria who suffer from cutaneous photosensitivity and abnormal liver function have illnesses of unknown etiology, highlighting our incomplete understanding of this complex condition.

Erythropoietic protoporphyria (EPP) is a disorder characterized by the pathological accumulation of a late heme biosynthetic intermediate, protoporphyrin IX (PPIX), in erythroid cells. Approximately 90% of patients with EPP carry a partial deficiency in *FECH* (EC 4.99.1.1, OMIM 177000), the gene for the mitochondrial enzyme ferrochelatase, which catalyzes the insertion of iron into PPIX for the final step in heme production. In most cases, EPP is due to cosegregation of a heterogeneous, family-specific deleterious *FECH* allele in compound heterozygosity with the common, low-expression, c.315–48C *FECH* allele, which affects the use of a cryptic splice-acceptor site in *FECH* pre-mRNA (4–6). A second, less common class of EPP results from gain-of-function mutations in *ALAS2*, the erythroid-specific gene for δ-aminolevulinate synthase (ALAS; EC 2.3.1.37, OMIM

300752), which catalyzes the initial step in heme biosynthesis. These dominant, gain-of-function *ALAS2* alleles increase ALA production, which triggers the accumulation of downstream heme precursors, especially PPIX. The proportion of patients with EPP with an *ALAS2* mutation is <5% in Europe (4, 5) and <10% in the United States (2). Importantly, genetic analysis fails to detect *FECH* and *ALAS2* mutations in 1–5% of families with a member with EPP (which are mostly homozygous for the WT FECH c.315–48T allele), suggesting involvement of loci other than *FECH* and *ALAS2* in this important metabolic illness (3, 7).

Significance

Although heme synthesis is ubiquitous, specific regulatory mechanisms couple heme production to cellular demand and environmental conditions. The importance of these regulatory mechanisms is highlighted by clinical variability in porphyrias caused by loss-of-function mutations in heme synthesis enzymes. Heme synthesis is also controlled by the mitochondrial AAA+ unfoldase ClpX, which participates in both heme-dependent degradation of δ-aminolevulinate synthase (ALAS) and ALAS activation. This study reports a human familial mutation in *CLPX* that contributes to erythropoietic protoporphyria (EPP) by partially inactivating CLPX. Reduced CLPX activity increases ALAS post-translational stability, causing pathological accumulation of protoporphyrin IX (PPIX) in human patients. Our results thus identify an additional gene that promotes PPIX overproduction and EPP and highlight the complex gene network contributing to disorders of heme metabolism.

Here, we report the identification of a third mechanism underlying EPP in an affected family. This EPP is promoted by a mutation in *CLPX*, which encodes an AAA+ (ATPases associated with various cellular activities) protein unfoldase. ClpX is widely conserved among bacteria and in the eukaryotic mitochondrion. ClpX works as a ring-shaped homohexamer and is best understood in its function in a proteasome-like complex with the peptidase ClpP (i.e., the ClpXP ATP-dependent protease). For well-studied examples of ClpXP substrates in bacteria, ClpX recognizes specific short sequence motifs in the substrate protein. ClpX unfolds the tertiary structure of substrate protein by ATP-powered polypeptide translocation through its central pore and then presents this unfolded sequence directly into the ClpP proteolytic chamber (reviewed in ref. 8). Recently, ClpX has been identified as a modulator of heme biosynthesis by activating ALAS (9), and also has been observed to mediate the turnover of ALAS under heme-replete conditions; this turnover requires a heme-binding motif in ALAS (10).

Here, we report the identification and analysis of a dominant heterozygous mutation that disables the ATPase activity of CLPX, causing accumulation of PPIX in red blood cells and promoting the development of EPP symptoms. Our experiments demonstrate how this impaired CLPX activity causes deleterious effects in heme metabolism, organismal physiology, and human health.

Results

An EPP-Affected Family Carries a Dominant CLPX Allele. We recently identified a family from Northern France in which the proband suffers from EPP of unknown etiology (Fig. 1A). The proband, an 18-y-old Caucasian female, was referred to the French Center of Porphyria because of early-onset (9 mo) acute photosensitivity, characterized by painful phototoxic reactions and elevated levels of free and zinc-chelated erythroid PPIX, phenotypes suggestive of EPP (Table 1). At the time of diagnosis, she also presented with a microcytic iron-deficiency anemia (Table 1). Her ferrochelatase (FECH) activity was normal. Furthermore, she did not carry any of the known gain-of-function mutations in the *ALAS2* gene that lead to EPP. No point mutations or large *FECH* gene deletions on chromosome 18 (3), where the *FECH* gene is located, were identified by linkage and comparative genomic hybridization array analysis (*SI Appendix*, Fig. S1). Moreover, she did not harbor the c.315–48C *FECH* low-expressed allele (4). Taken together, these data demonstrate that the proband has an unusual form of EPP (Table 1). Among the proband's family members, her father (II.4) and uncle (II.2) also presented with free and zinc-PPIX accumulation in erythrocytes and associated mild photosensitivity, but without the complete clinical symptoms of EPP (Fig. 1A and Table 1).

After linkage analysis and exclusion of candidate genes (*SI Appendix*, Table S1), whole-exome sequencing revealed that the proband (III.2) carried a single nucleotide substitution (g.27511 G > A) at the exon 7 splice junction border in one of her two *CLPX* alleles (Fig. 1B). This mutation was not present in 126,216 control reference exomes queried in the genome aggregation database (gnomad.broadinstitute.org), suggesting that it is not a common human polymorphism. To establish the inheritance pattern of this mutation, we performed Sanger sequencing of gDNA obtained from whole blood of the proband's relatives and collected clinical data from these family members. Among nuclear family members, only the proband's father (II.4) and uncle (II.2) harbored the identical heterozygous *CLPX* mutation (Fig. 1A). Thus, the G > A transition in *CLPX* cDNA was fully segregated with the PPIX accumulation and was inherited in a pattern consistent with Mendelian dominance. The pre-mRNA from the mutant allele was normally spliced (Fig. 1C), and the mutation was predicted to encode the single amino acid p.Gly298Asp substitution in the mature CLPX protein (CLPX^{GD}). Thus, we propose that this *CLPX* mutation increases PPIX production with incomplete penetrance for full EPP; disease
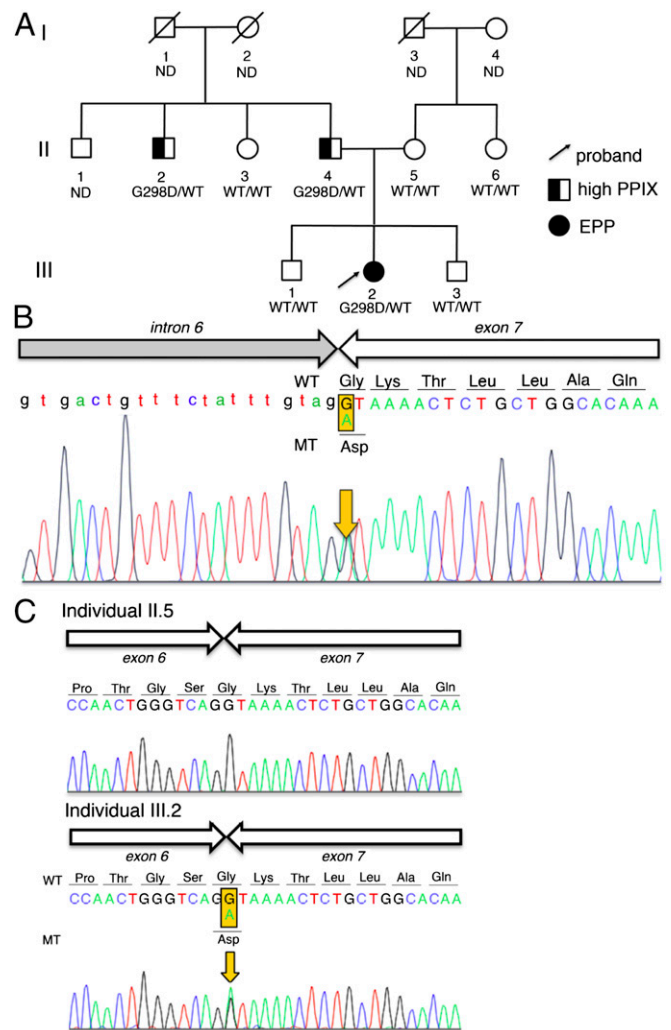
Fig. 1. Sequencing identifies mutations in *CLPX*. (*A*) Mendelian dominant inheritance segregation of PPIX overproduction was observed in the proband's family. The proband is indicated by an arrow. (*B*) Sequencing revealed a single nucleotide substitution in CLPX (g.27511 G > A) in genomic DNA from the proband (III.2). (*C*) Sequencing of cDNA revealed a single nucleotide substitution (c.1102 G > A) in the proband, but not in her mother (II.5), resulting in a p.Gly298Asp missense mutation (CLPX^{GD}). *CLPX^{GD}* mRNA is normally spliced.

progression and severity are likely influenced by environmental conditions and/or genetic modifiers. Consequently, we went on to explore the molecular mechanism by which this *CLPX* mutation alters heme metabolism and contributes to EPP.

CLPX^{GD} Has a Defective ATPase Active Site. Human CLPX glycine 298 is a highly conserved residue in the Walker A motif (Fig. 2A). This motif forms part of the ATP-binding pocket and participates in the positioning and hydrolysis of ATP (reviewed in ref. 8). The G298D mutation is predicted to prevent ATP binding by steric occlusion or distortion of the active site (Fig. 2B); thus, we sought to determine whether the *CLPX* G298D mutation in our pedigree caused EPP by disrupting the regulatory function(s) of CLPX on heme synthesis. To determine the consequence of the G298D mutation on CLPX activity, we assayed ATPase activity of wild-type (WT) murine CLPX and a G298D CLPX variant (CLPX^{GD}) in vitro. CLPX^{GD} lacked detectable ATPase activity and partially suppressed the ATPase of WT CLPX protomers (Fig. 2C), suggesting that the dominant-negative phenotype of the mutant allele could be caused by

Table 1. Biochemical data in affected subjects of the EPP family under study

Heme- and iron-related biochemical markers	Reference*	II.2	II.4	III.2
Total porphyrins in plasma, nmol/L	<20	52	64	936
Erythroid PPIX, μmol/L RBC	<1.9	26.7	30.4	140.9
Free PPIX, %	<28	38	33	71
ZnPPIX, %	>72	62	67	29
FECH activity, nmol/mg protein/h	>3.5	4.5	4.4	3.6
Hemoglobin, g/dL	12–16	15.9	15.5	11.5
Iron, μmol/L	12–26	20	25	4
Transferrin saturation, %	20–45	32	31	5
Soluble transferrin receptor, mg/L	0.76–1.76	1.25	1.41	3.95
Ferritin, μg/L	15–250 (males)	171	196	5
	8–150 (females)			

All three individuals carrying one copy of the $CLPX^{GD}$ allele had significantly elevated total porphyrin, erythroid protoporphyrin, and free PPIX levels. Their FECH activities were normal. The proband (III.2) exhibited symptoms of iron deficiency, with decreased iron, transferrin saturation, and ferritin levels, but this phenotype did not cosegregate with the mutation.
*Reference values obtained from Ducamp et al. (14).

heterooligomerization of WT and mutant CLPX subunits. Suppression of WT CLPX ATPase activity by $CLPX^{GD}$ plateaued at a ~30% reduction in activity, indicating that WT CLPX protomers within any heterooligomers retain partial activity.

$CLPX^{GD}$ Increases ALAS and PPIX Levels in Vivo. To determine whether $CLPX^{GD}$ could induce erythropoietic porphyria, we transiently expressed FLAG-tagged CLPX and $CLPX^{GD}$ in HEK293T cells (Fig. 3A). HEK293T cells that expressed $CLPX^{GD}$ contained ~1.5-fold more PPIX than control or CLPX-expressing cells (Fig. 3B). Because CLPX modulates ALAS activity (9, 10), which in turn can alter downstream PPIX levels, we analyzed ALAS activity in CLPX-expressing cells. In HEK293T fibroblasts, expression of CLPX decreased endogenous ALAS1 activity (Fig. 3C), and this CLPX effect also lowered ALAS1 protein levels (Fig. 3A). In contrast, the expression of $CLPX^{GD}$ resulted in increased activity of ALAS1 (Fig. 3C) and a parallel increase in the level of ALAS1 protein (Fig. 3A). Furthermore, consistent with the findings reported by Kubota et al. (10), CRISPR-mediated disruption of CLPX in K562 cells also caused an increase in ALAS1 protein levels (*SI Appendix*, Fig. S2).

Expression of $CLPX^{GD}$ in Friend mouse erythroleukemia (MEL) cells (Fig. 3D) similarly increased PPIX production (Fig. 3E) and increased ALAS2 activity (Fig. 3F). Likewise, we observed that the expression of $CLPX^{GD}$ increased ALAS2 protein levels, whereas expression of CLPX decreased ALAS2 levels (Fig. 3D). Interestingly, the decrease in ALAS2 protein caused by $CLPX^{GD}$ expression did not change the total ALAS activity measured (Fig. 3F).

To determine whether $CLPX^{GD}$ similarly increased ALAS activity in an animal model, we injected equal amounts of cRNA encoding FLAG-tagged CLPX and $CLPX^{GD}$ into zebrafish embryos. The injected *CLPX* and *CLPX^{GD}* cRNA was efficiently translated into CLPX protein (Fig. 3G). $CLPX^{GD}$ expression caused an approximately twofold increase in ALAS activity (Fig. 3H), consistent with cell culture data.

We observed similar increases in ALAS protein levels and activity in patient-derived cells as in $CLPX^{GD}$-expressing cell and animal models. ALAS1 levels (Fig. 4A) and activity (Table 2) were elevated, as demonstrated by accumulation of the ALA metabolite in EBV-immortalized lymphoblastoid cells obtained from $CLPX^{WT/GD}$ individuals. Modestly increased ALAS2 levels were also found in erythroid cells obtained from differentiation of primary CD34+ hematopoietic stem cells from the index cases (Fig. 4B). Taken together, our data demonstrate that expression of $CLPX^{GD}$ in cell cultures and zebrafish phenocopies the *CLPX^{GD}* effect in patient cells, causing increased ALAS protein, higher ALA levels, and thus accumulation of PPIX, the biochemical hallmark of EPP.

$CLPX^{GD}$ Slows ALAS Degradation in Vivo. An attractive hypothesis to explain how $CLPX^{GD}$ causes PPIX accumulation is that the reduced activity of mixed hexamers of WT CLPX and $CLPX^{GD}$ reduces the rate of CLPX-dependent degradation of both ALAS1 (10) and ALAS2. Thus, we assessed whether $CLPX^{GD}$ increased ALAS activity by increasing the stability of the ALAS
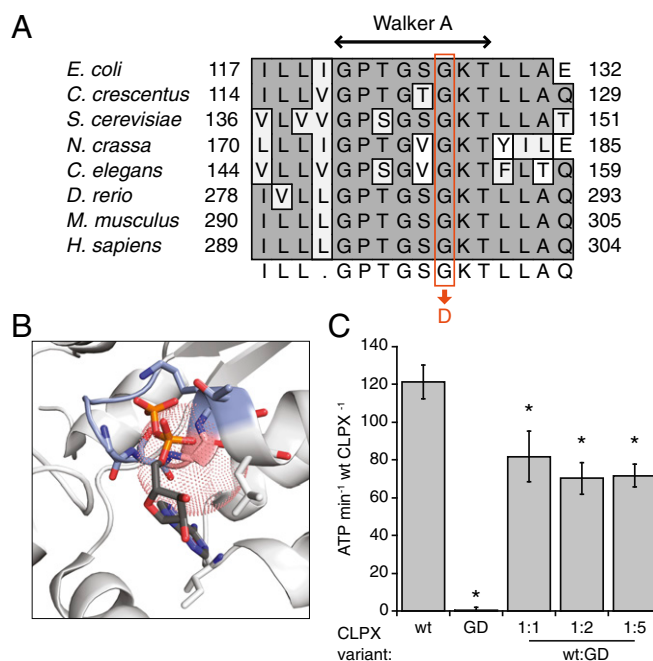
Fig. 2. The *CLPX^{GD}* mutation compromises the ATPase active site structure and activity. (A) The *CLPX^{GD}* mutation occurs in the highly conserved Walker A ATPase motif. (B) Rendering of a nucleotide-binding pocket of ClpX (light gray) with the Walker A motif (blue-gray) and the residue corresponding to *H. sapiens* CLPX Gly298 (salmon). Coordinates are from a structure of *E. coli* ClpX$_6$ bound to ADP (PDB ID code 3HWS) (38). The dotted sphere represents the maximum extension of an aspartate side chain from this position (3.72 Å). ADP atoms are colored using the standard scheme, and side chain residues that form hydrogen bonds with ADP are also shown. (C) ATPase activity of CLPX, $CLPX^{GD}$, and mixtures thereof. ATPase activity of 0.15 μM (hexamer concentration) CLPX (WT), 0.15 μM $CLPX^{GD}$ (GD), or 0.15 μM CLPX plus 0.15, 0.3, or 0.75 μM $CLPX^{GD}$ (WT + GD) is displayed. Activity is calculated relative to the concentration of WT CLPX in each condition (ATP per minute per WT CLPX$_6$). Mean values ± SD are plotted; $n \geq 3$ biological replicates. *Reduced activity, $P \leq 0.005$, Student's t test.
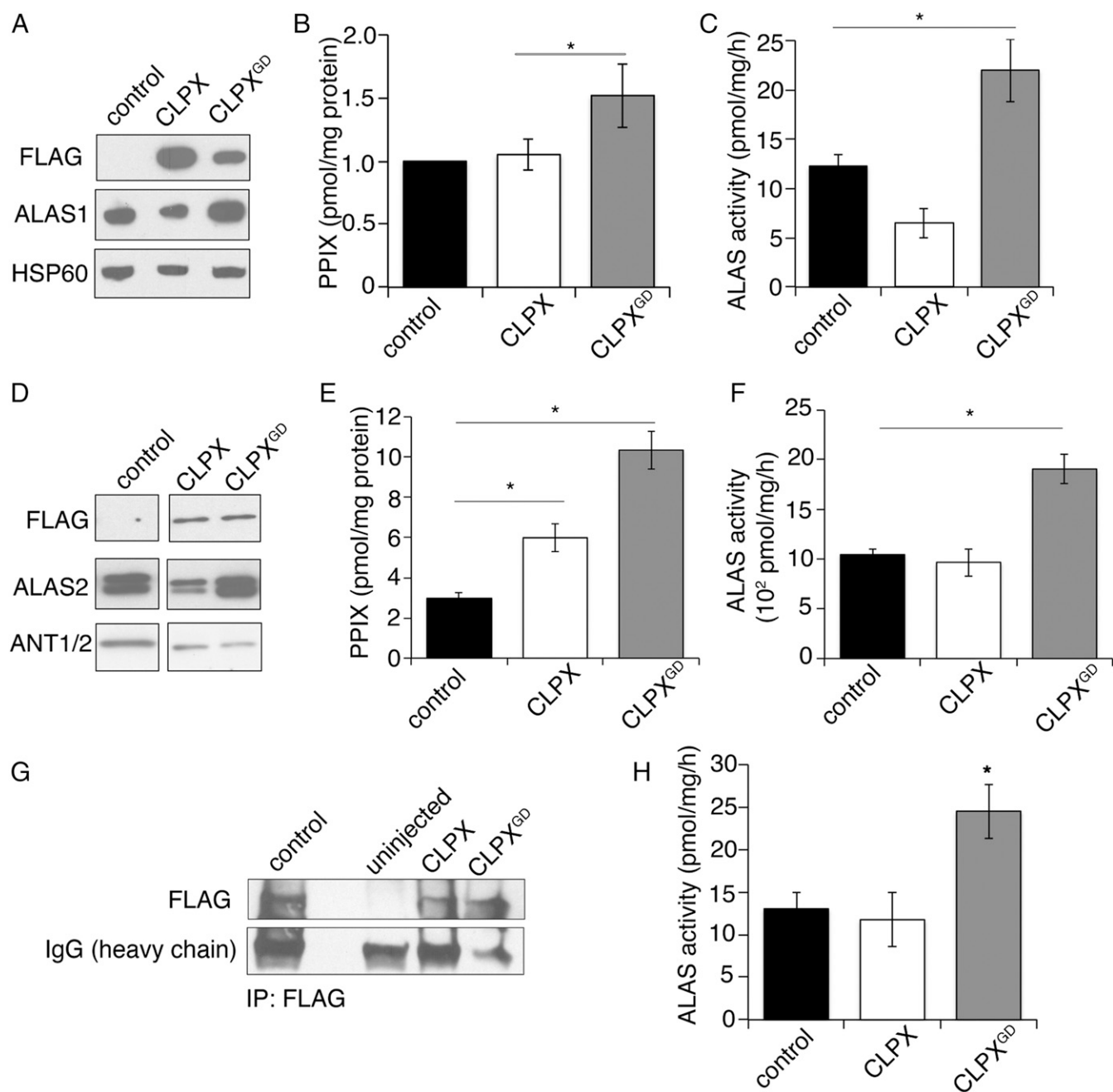
Fig. 3. Expression of CLPX[GD] causes increased ALAS activity and increased PPIX. (*A*) Western blot analysis of mitochondrial lysates from HEK293T cells expressing C-terminal FLAG-tagged CLPX or CLPX[GD]. (*B*) HPLC analysis of PPIX levels in HEK293T cells. (*C*) HPLC analysis of ALAS1 activity in HEK293T cells. (*D*) Western blot analysis of MEL cells stably expressing C-terminal FLAG-tagged CLPX or CLPX[GD]. (*E*) HPLC analysis of PPIX levels in MEL cells. (*F*) HPLC analysis of ALAS2 activity (ALA production) in MEL cells. (*G*) Western blot analysis of FLAG immunoprecipitation from lysates from uninjected and either CLPX-FLAG or CLPX-FLAG[GD] cRNA-injected zebrafish embryos. (*H*) ALAS activity was assayed by HPLC from zebrafish embryos described in *G*. Mean values ± SEM are plotted; $n > 3$. *$P < 0.05$, Student's *t* test.

proteins. We monitored the rate of ALAS1 and ALAS2 turnover in cultured cells by Western blot analysis following inhibition of protein synthesis. In brief, we treated CLPX- or CLPX[GD]-expressing HEK293T cells with cycloheximide (CHX) to inhibit de novo translation (11–15), and monitored the decrease in ALAS1 or ALAS2 protein over several hours by Western blot analysis. ALAS1 degradation was slow specifically in cells expressing CLPX[GD] (Fig. 4 *C* and *D*, *Left*). Interestingly, CLPX[GD] itself was less stable than CLPX (Fig. 4 *C* and *D*, *Right*). ALAS2 degradation was also decreased by expression of CLPX[GD] in differentiating MEL cells (Fig. 4 *E* and *F*). Therefore, impaired

CLPX-dependent turnover of ALAS could explain the alterations in both housekeeping and erythroid-specific heme synthesis caused by the presence of heterozygous *CLPX[GD]* and *CLPX[WT]* alleles.

Assembly of CLPX-CLPX[GD] Heteromeric CLPX Unfoldase and CLPXP Protease. Previous work with *Escherichia coli* and human homologs of ClpX and ClpP has demonstrated that ATP binding stabilizes ClpX hexamers and is essential for ClpXP complex formation (16–18). Given the effect of the G298D mutation on the ATPase active site of ClpX, we believed it important to
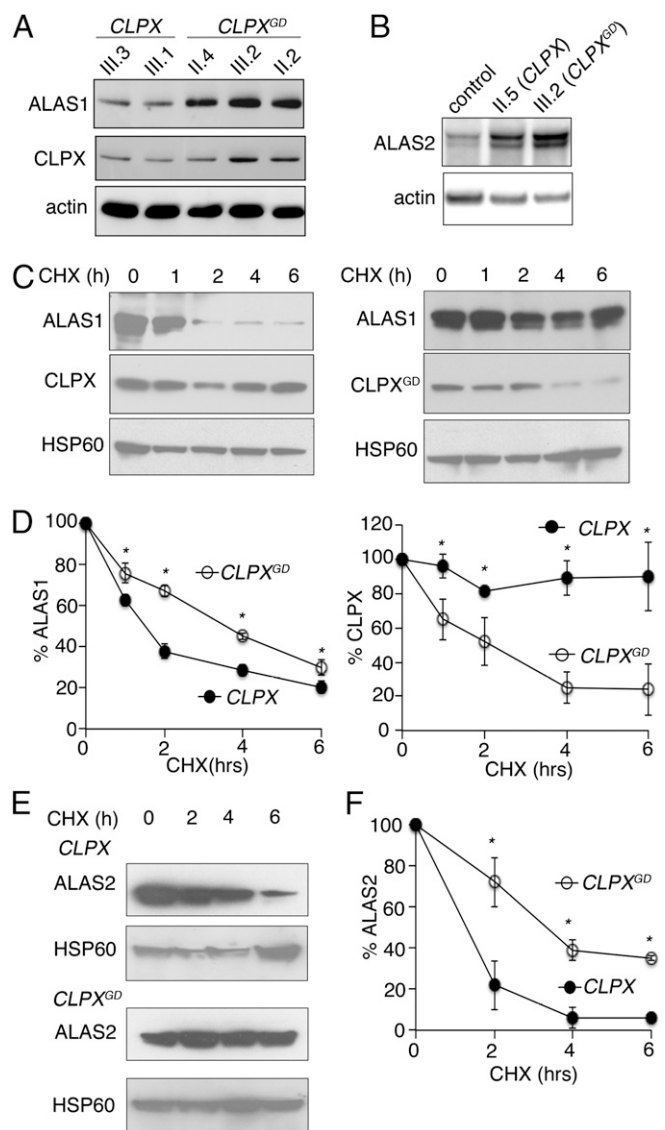
Fig. 4. Expression of CLPX[GD] mutant stabilizes ALAS protein. (*A*) Western blot analysis of immortalized lymphoblastoid cells obtained from the proband and her family members (Fig. 1*A*) showed increased levels of ALAS1 protein in individuals carrying a *CLPX[GD]* allele (II.4, III.2, and II.2) compared with unaffected family members (III.3 and III.1). (*B*) Western blot analysis of patient-derived primary CD34$^+$ hematopoietic stem cells differentiated to erythroid cells. (*C*) CHX block of protein translation in HEK293 cells (cells as described in Fig. 3*A*), followed by Western blot analysis of mitochondrial lysates collected after treatment. (*D*, *Left*) Quantification of ALAS1 degradation after CHX treatment. Both bands, corresponding to the precursor (upper band) and mature (lower band) forms of ALAS1 were quantified. Quantification of CLPX and CLPX[GD] degradation after CHX treatment. Both proteins were normalized to HSP60 expression (*n* = 3). (*E*) Western blot analysis of time course following CHX treatment in MEL cells expressing CLPX or CLPX[GD]. (*F*) Quantification of ALAS2 degradation in *E*. ALAS2 was normalized to HSP60 expression. Mean values ± SEM are plotted; *n* > 3. *$P < 0.05$, Student's *t* test.

directly test the ability of CLPX[GD] to coassemble with WT CLPX and with CLPP. Thus, we tested complex formation among these purified protein variants. We found that the interaction of CLPX[GD] with WT CLPX protomers was not substantially perturbed, as assessed by coimmunoprecipitation (co-IP) (Fig. 5*A*). On analysis of CLPX-CLPP complex formation by CLPP pull-down, WT CLPX was pulled down by CLPP in at ATP-dependent manner, whereas CLPX[GD] was not pulled down by CLPP (Fig.

5*B*), as predicted because of its defective ATP-binding site. In an equimolar mixture of CLPX[GD] and WT CLPX, however, both CLPX variants coisolated with CLPP, but the total amount of CLPX recovered was reduced to half of that recovered from the WT CLPX-only condition. (Fig. 5*B*). These findings indicate that mixed hexamers composed of WT and G298D CLPX interact more weakly with CLPP than fully WT CLPX hexamers. Therefore, along with reducing the ATPase activity of CLPX in the cell, CLPX[GD] likely also reduces the abundance and degradation activity of CLPXP complexes in vivo. If CLPXP directly degrades the ALAS proteins, then this weakened CLPX-CLPP interaction would be expected to contribute to the reduced ALAS1 and ALAS2 turnover that we observe.

Discussion

Previous work has shown that ClpX activates ALAS by accelerating incorporation of the essential ALAS cofactor, pyridoxal 5'-phosphate (PLP) (9). Knockdown of one of two ClpX homologs in zebrafish, *clpxa*, caused an erythropoietic anemia that was chemically complemented by the addition of ALA, indicating that this anemia was due to reduced ALAS activity (9). Furthermore, in this previous study, the CLPXP proteolytic complex was not observed to degrade ALAS2 in vitro. The data reported here and by Kubota et al. (10) suggest that additional factors, such as autoregulatory free heme or collaboration with the Lon protease (19), may be required for CLPX-mediated degradation of ALAS.

Based on our present results, we suggest a model that integrates both mechanisms by which ClpX modulates ALAS activity, acceleration of PLP cofactor incorporation (activation), and promotion of ALAS protein turnover (degradation) (Fig. 5*C*). The balance of these mechanisms in vivo determines whether stimulation or suppression of ALAS activity by CLPX is observed. When CLPX is absent or expressed at only a low level, both ALAS activation and degradation are strongly blocked, causing an accumulation of ALAS with decreased enzymatic activity and thus reduced ALA synthesis, causing anemia (Fig. 5*C*, *Right*). In the present study, *CLPX[WT/GD]* heterozygous individuals contain CLPX[WT/GD] heteromeric complexes with reduced ATPase activity and weakened interaction with CLPP. The resulting reduction in ALAS degradation has a stronger phenotypic consequence than possible decreased activation, likely due in part to the weaker interaction of CLPX[WT/GD] heterohexamers with the CLPP peptidase, resulting in a net increase in ALA and PPIX (Fig. 5*C*, *Middle*). Furthermore, it is well established with bacterial ClpXP that the unfolding of some protein substrates requires much more ATP and a higher ClpX-ATPase rate compared with other proteins, and the differences depend on the specific structure of the substrate protein (reviewed in ref. 20). The mixed CLPX[WT/GD] enzyme may be more defective in the complete ALAS unfolding required for degradation than in the limited unfolding that we proposed is required for activation (9). Thus, when cells contain CLPX[WT/GD] heterohexamers, active, intact ALAS accumulates. Cellular FECH activity and iron levels are insufficient to convert the resulting excess PPIX to heme, causing cells to accumulate free and zinc-PPIX and leading to symptoms of porphyria.

Table 2. ALA metabolite levels (arbitrary units/g protein) in lymphoblastoid cells obtained from *CLPX[WT/WT]* and *CLPX[WT/GD]* individuals
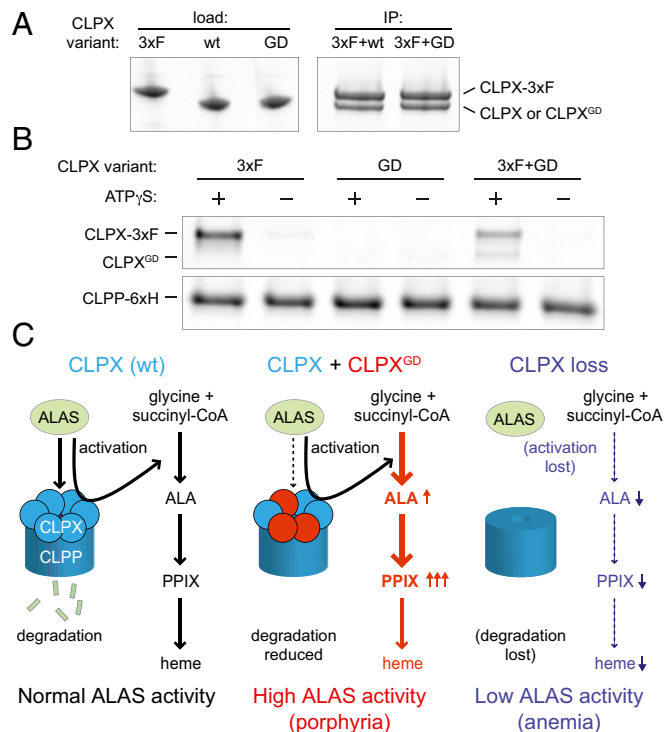
CLPX[WT/WT]		CLPX[WT/GD]		
III.1	III.3	II.2	II.4	III.2
14.9	20.6	37.1	23.8	43.9

CLPX[WT/GD] individuals exhibit elevated levels of the ALA metabolite.

The pedigree of the proband's family clearly demonstrates the dominant coinheritance of PPIX accumulation with the $CLPX^{GD}$ allele through vertical transmission over two generations (Fig.1 and *SI Appendix*, Fig. S3). Human dominantly inherited diseases are often characterized by incomplete penetrance and variable presentation of disease symptoms, usually due to differences in the influence of environmental factors and/or modifier genes on different individuals. Our data suggest that the human dominant *CLPX* disorder behaves in this manner, as observed for the previously reported dominant porphyrias (1). Thus, we have

Fig. 5. CLPX and CLPXP assembly and models of the disease mechanism. (*A*) Coimmunoprecipitation of purified murine CLPX variants to assess heterooligomerization of WT and G298D variants. 3xFLAG-tagged ClpX was immunoprecipitated from a mixture with untagged CLPX or CLPX^{GD}. The precipitate was separated by SDS/PAGE and stained with Sypro Orange. (*B*) Pull-down to assess the interaction of CLPX variants (WT or G298D) with CLPP-His$_6$. 3xFLAG-tagged WT CLPX was used to distinguish it from CLPX^{GD}. CLPX were incubated with CLPP-His$_6$ and His-Tag Dynabeads in the presence or absence of 2.5 mM ATPγS. Coisolated proteins were separated by SDS/PAGE and stained with Sypro Red. With ATPγS, total pull-down of CLPX with CLPP in the mixed WT and G298D CLPX sample was 0.5 ± 0.1 relative to WT CLPX; no significant association of CLPX^{GD} alone with CLPP was observed. $P = 0.002$ (Student's t test, n of 3) for reduced pull-down of mixed WT CLPX and CLPX^{GD} with CLPP. (*C*) Models of CLPX regulation of ALAS. (*Left*) Under normal circumstances, CLPX (blue circles) degrades ALAS in complex with CLPP (dark-blue cylinder), keeping ALA levels in check, preventing PPIX from accumulating (10). Concurrently, CLPX activates ALAS by promoting PLP incorporation (9). Note that direct degradation by CLPXP of ALAS1 or ALAS2 has not been demonstrated in vitro, and the influence of CLPX on ALAS stability could be more complex. (*Middle*) In a CLPX$^{WT/GD}$ heterozygote, CLPX^{GD} (red circles) heterooligomerizes with CLPX, to form a dominant inhibitor of the ATPase activity of the hexamer. The resultant CLPXP complex is deficient in proteolytic activity, leading to an accumulation of ALAS that is more severe than any deficiency in PLP incorporation. (Any defect in ALAS activation by the heterohexameric CLPX has not been quantified, but likely is less impaired than in ALAS degradation; see text). This combination results in abnormally high ALAS activity and accumulation of PPIX, contributing to EPP. (*Right*) When CLPX is lost, reduced activation of ALAS is phenotypically stronger than increased ALAS protein, leading to decreased ALA production and anemia (9).

uncovered a new molecular basis for EPP, a defect in the AAA+ unfoldase CLPX that results in aberrant control of the key heme synthetic enzyme ALAS.

Given the contribution of ClpX and ClpXP to essential organismal processes such as heme synthesis (9, 10) and mitochondrial respiration (21, 22), it is likely that *CLPX* mutations contribute to additional mitochondriopathies and metabolic disorders. Causative recessive mutations in *CLPP* have been identified in Perrault syndrome (23, 24). Because no unfoldase-independent role of ClpP is known or predicted, CLPX activity is likely required for the CLPP function(s) that are perturbed in Perrault syndrome. *CLPX* mutations also could contribute to sideroblastic anemia by slowing PLP incorporation into ALAS2, phenocopying XLPP caused by ALAS2 mutations that inhibit PLP binding (25–28). Treatment with large doses of vitamin B6 (to yield PLP) might bypass a deficiency in CLPX-stimulated PLP incorporation into ALAS2 in a manner analogous to treatment of patients with XLPP with B6-responsive *ALAS2* mutations. Because the genetic variant of EPP reported here shares more similarities with *ALAS2*-based EPP (XLPP) than with *FECH*-based EPP, it could be helpful to treat patients with CLPX-based EPP with supplemental iron to convert excess PPIX to heme, as has been beneficial for patients with XLPP with a normal *FECH* gene (3, 29). The incomplete EPP penetrance and variable clinical symptoms observed among the $CLPX^{GD}$-carrying individuals may be based in environmental factors. In EPP, whether iron therapy is effective or might even sometimes worsen the disease is a matter of debate (30, 31); however, recent work suggests that iron status can modulate the phenotype both in congenital erythropoietic porphyria (32) and in XLPP (3, 5, 29). Therefore, we speculate that the iron deficiency of the index $CLPX^{GD}$ patient may result from an independent pathological process that contributes to the penetrance of EPP. It is our hope that further understanding of the complex network of enzyme and cofactor interactions controlling heme synthesis will continue to contribute ideas for therapeutic strategies to treat diseases caused by aberrant regulation of heme metabolism.

Materials and Methods

Human and Vertebrate Animal Study Approval. The study was approved by local Ethics Committees in accordance with the ethical principles for medical research involving human subjects and its subsequent amendments of the Declaration of Helsinki (R162-16–7 and 145–15-4, French ethical agreement). All family members provided written informed consent, and the European Union Institutional Review Board at INSERM approved the protocols. Vertebrate animal studies were performed in compliance with Institutional Animal Care and Use Committee protocols at Boston Children's Hospital, Brigham & Women's Hospital, and MIT.

Biochemical Analysis. The diagnosis of EPP was based on biochemical analyses of porphyrins in plasma, feces, and erythrocytes, and on FECH enzymatic assays performed according to the European Porphyria Network (EPNET) guidelines and quality control schemes (porphyria.eu/). Erythroid porphyrins were measured as described previously (33). The percentage of zinc-protoporphyrin was calculated from fluorescence emission spectra of extracted of erythrocyte hemolysates. Porphyrins were extracted as described previously (34) and analyzed by HPLC (35). Intracellular ALA levels were measured by LC-MS/MS (UPLC-Xevo TQMS; Waters). Cells were sonicated in the presence of 1 mM succinylacetone, and samples were pretreated by solid-phase extraction using MCX columns (Waters). PPIX in HEK293T and MEL cells and ALAS activity were quantified as described previously (36, 37).

Cell Culture and Metabolite Analysis. Lymphoblastoid cells were obtained from the Biological Resource Center, Hôpital Cochin-APHP (Assistance Publique-Hôpitaux de Paris). They were cultured in RPMI 1640 medium (Gibco) supplemented with 10% FBS, 2% L-glutamine 200 mM, 10 mM Hepes, and antibiotics (100 U/mL penicillin and 100 μg/mL streptomycin). *CLPX* genotypes were identified by Sanger sequencing (*SI Appendix*, Fig. S3). DS19 MEL clones were a gift from Arthur Skoultchi (Albert Einstein College of Medicine), and the Biological Resource Center at Hôpital Cochin-APHP generously established the lymphoblastoid cell lines.

Mononuclear cells were isolated by Ficoll density-gradient centrifugation (PAA Laboratories) from 60 mL of peripheral whole blood. CD34$^+$ cells were purified using immunomagnetic beads (MACS CD34$^+$ MicroBead Kit; Miltenyi Biotec). CD34$^+$ cells were differentiated into erythroid cells by culture in Iscove's Modified Dulbecco's Medium (Gibco) supplemented with 15% BIT 9500 (Stemcell Technologies), 2 U/mL EPO, 100 ng/mL SCF, 10 ng/mL IL-6, and 10 ng/mL IL-3 (Miltenyi Biotec), MEL (DS19 subclone) cells were differentiated by incubation in complete DMEM supplemented with 2% DMSO for 3 d. To assess hemoglobinization, o-dianisidine staining was performed as described previously (36).

Immunoprecipitation and Western Blot Analysis. Zebrafish embryos at 24 h postfertilization with eGFP expression were lysed in groups of ~50 embryos in RIPA buffer/protease inhibitor mixture (Roche) by dounce. The clarified soluble lysate after centrifugation was immunoprecipitated with anti-FLAG agarose beads (Sigma-Aldrich) for 12 h at 4 °C, after which immune complex beads were serially washed with PBST/protease inhibitor mixture (Roche) and eluted in boiling Laemmli loading solution. The eluted immune complex was resolved on SDS/PAGE and visualized by Western blot analysis.

The following antibodies were used for Western blot analysis: peroxidase-conjugated anti-FLAG M2 (Sigma-Aldrich), anti-ALAS1 (ab84962; Abcam), anti-ALAS2 (ab184964; Abcam or rabbit anti-human ALAS2; Agios Pharmaceutical), anti-CLPX (AP1067b; Abgent), anti-HSP60 (Santa Cruz Biotechnology), anti-ANT (Santa Cruz Biotechnology), and anti–β-actin (Sigma-Aldrich).

CHX Block. Inhibition of translation was carried out with 100 μg/mL CHX (Sigma-Aldrich) as described previously (11). Cells were harvested at indicated times after CHX treatment. Proteins obtained from whole-cell lysates (HEK293T cells) or mitochondrial fractions (MEL cells) were resolved by SDS/PAGE. ALAS1, ALAS2, and CLPX were detected by Western blot analysis, and protein levels were quantified using ImageJ (37).

CLPX Biochemistry. Murine CLPX variants and human CLPP$_{His6}$ were expressed and purified as described previously (9). Bacterial expression vectors for the CLPX^{GD} and CLPX-3xFLAG proteins were generated by site-directed mutagenesis and isothermal assembly, respectively, of the previously reported CLPX expression vector. CLPX ATPase activity was monitored at 30 °C by the decrease in absorbance at 340 nm in an NADH-coupled assay (2.5 mM ATP, 1 mM NADH, 7.5 mM phosphoenolpyruvate, 20 U/mL lactate dehydrogenase, and 20 U/mL pyruvate kinase) in 25 mM Hepes pH 7.6, 100 mM KCl, 5 mM MgCl$_2$, and 10% glycerol.

Co-IP of purified CLPX-3xFLAG and CLPX variants was performed with FLAG M2 antibody-conjugated magnetic agarose beads (Sigma-Aldrich). Here 0.25 μM CLPX-3xFLAG and 0.25 μM CLPX or CLPX^{GD} were incubated in 25 mM Hepes pH 7.6, 100 mM KCl, 5 mM MgCl$_2$, 10% glycerol, 0.1% Triton

X-100, 0.5 mg/mL acetylated BSA, and 1 mM DTT with 12 μL of beads in a 50-μL total volume on ice for 45 min with intermittent gentle mixing. Beads and bound proteins were washed three times in binding buffer and eluted on ice for 45 min with 30 μL of 1 mg/mL 3xFLAG peptide in binding buffer. Eluted proteins were separated by SDS/PAGE, stained with Sypro Orange, and imaged with a Typhoon FLA 9500 scanner (GE Healthcare). Coisolation of CLPX variants with human CLPP$_{His6}$ was performed using His-Tag Dynabeads (Thermo Fisher Scientific) in the same buffer used for anti-FLAG co-IP, except for the addition of 10 mM imidazole. CLPX variants were mixed together as indicated, and CLPP$_{His6}$ and ATPγS were added as indicated. The mixtures were incubated for 10 min at room temperature. His-Tag Dynabeads were added in an equal volume of buffer to yield a concentration of 0.3 μM total CLPX hexamer (CLPX-3xFLAG, CLPX^{GD}, or an equimolar mixture of both) and 0.3 μM CLPP 14-mer in 30 μL. The mixtures were incubated for 10 min at room temperature with intermittent gentle mixing. Beads and bound proteins were washed three times with binding buffer, then eluted for 10 min at room temperature in 30 μL of binding buffer with 300 mM imidazole. Eluted proteins were separated by SDS/PAGE, stained with Sypro Red, and imaged with a Typhoon FLA 9500 scanner (GE Healthcare).

1. Puy H, Gouya L, Deybach J-C (2010) Porphyrias. *Lancet* 375:924–937.
2. Balwani M, Desnick RJ (2012) The porphyrias: Advances in diagnosis and treatment. *Blood* 120:4496–4504.
3. Landefeld C, et al. (2016) X-linked protoporphyria: Iron supplementation improves protoporphyrin overload, liver damage and anaemia. *Br J Haematol* 173:482–484.
4. Whatley SD, et al. (2007) Gene dosage analysis identifies large deletions of the FECH gene in 10% of families with erythropoietic protoporphyria. *J Invest Dermatol* 127:2790–2794.
5. Whatley SD, et al. (2008) C-terminal deletions in the ALAS2 gene lead to gain of function and cause X-linked dominant protoporphyria without anemia or iron overload. *Am J Hum Genet* 83:408–414.
6. Gouya L, et al. (1996) Modulation of the phenotype in dominant erythropoietic protoporphyria by a low expression of the normal ferrochelatase allele. *Am J Hum Genet* 58:292–299.
7. Whatley SD, Badminton MN (2013) Role of genetic testing in the management of patients with inherited porphyria and their families. *Ann Clin Biochem* 50:204–216.
8. Baker TA, Sauer RT (2012) ClpXP, an ATP-powered unfolding and protein-degradation machine. *Biochim Biophys Acta* 1823:15–28.
9. Kardon JR, et al. (2015) Mitochondrial ClpX activates a key enzyme for heme biosynthesis and erythropoiesis. *Cell* 161:858–867.
10. Kubota Y, et al. (2016) Novel mechanisms for heme-dependent degradation of ALAS1 protein as a component of negative feedback regulation of heme biosynthesis. *J Biol Chem* 291:20516–20529.
11. Yien YY, Bieker JJ (2012) Functional interactions between erythroid Krüppel-like factor (EKLF/KLF1) and protein phosphatase PPM1B/PP2Cβ. *J Biol Chem* 287:15193–15204.
12. Quadrini KJ, Bieker JJ (2006) EKLF/KLF1 is ubiquitinated in vivo and its stability is regulated by activation domain sequences through the 26S proteasome. *FEBS Lett* 580:2285–2293.
13. Laghmani K, et al. (2016) Polyhydramnios, transient antenatal Bartter's syndrome, and *MAGED2* mutations. *N Engl J Med* 374:1853–1863.

14. Ducamp S, et al. (2013) Molecular and functional analysis of the C-terminal region of human erythroid-specific 5-aminolevulinic synthase associated with X-linked dominant protoporphyria (XLDPP). *Hum Mol Genet* 22:1280–1288.
15. Schneider-Poetsch T, et al. (2010) Inhibition of eukaryotic translation elongation by cycloheximide and lactimidomycin. *Nat Chem Biol* 6:209–217.
16. Kang SG, et al. (2002) Functional proteolytic complexes of the human mitochondrial ATP-dependent protease, hClpXP. *J Biol Chem* 277:21095–21102.
17. Martin A, Baker TA, Sauer RT (2007) Distinct static and dynamic interactions control ATPase-peptidase communication in a AAA+ protease. *Mol Cell* 27:41–52.
18. Joshi SA, Hersch GL, Baker TA, Sauer RT (2004) Communication between ClpX and ClpP during substrate processing and degradation. *Nat Struct Mol Biol* 11:404–411.
19. Tian Q, et al. (2011) Lon peptidase 1 (LONP1)-dependent breakdown of mitochondrial 5-aminolevulinic acid synthase protein by heme in human liver cells. *J Biol Chem* 286:26424–26430.
20. Olivares AO, Baker TA, Sauer RT (2016) Mechanistic insights into bacterial AAA+ proteases and protein-remodelling machines. *Nat Rev Microbiol* 14:33–44.
21. Seo JH, et al. (2016) The mitochondrial unfoldase-peptidase complex ClpXP controls bioenergetics stress and metastasis. *PLoS Biol* 14:e1002507.
22. Deepa SS, et al. (2016) Down-regulation of the mitochondrial matrix peptidase ClpP in muscle cells causes mitochondrial dysfunction and decreases cell proliferation. *Free Radic Biol Med* 91:281–292.
23. Gersch M, et al. (2016) Barrel-shaped ClpP proteases display attenuated cleavage specificities. *ACS Chem Biol* 11:389–399.
24. Jenkinson EM, et al. (2013) Perrault syndrome is caused by recessive mutations in CLPP, encoding a mitochondrial ATP-dependent chambered protease. *Am J Hum Genet* 92:605–613.
25. Furuyama K, et al. (1997) Pyridoxine refractory X-linked sideroblastic anemia caused by a point mutation in the erythroid 5-aminolevulinate synthase gene. *Blood* 90:822–830.
26. Cotter PD, Baumann M, Bishop DF (1992) Enzymatic defect in "X-linked" sideroblastic anemia: Molecular evidence for erythroid delta-aminolevulinate synthase deficiency. *Proc Natl Acad Sci USA* 89:4028–4032.

27. Cox TC, Bawden MJ, Martin A, May BK (1991) Human erythroid 5-aminolevulinate synthase: Promoter analysis and identification of an iron-responsive element in the mRNA. *EMBO J* 10:1891–1902.

28. Prades E, et al. (1995) A new mutation of the ALAS2 gene in a large family with X-linked sideroblastic anemia. *Hum Genet* 95:424–428.

29. Barman-Aksözen J, Minder EI, Schubiger C, Biolcati G, Schneider-Yin X (2015) In ferrochelatase-deficient protoporphyria patients, ALAS2 expression is enhanced and erythrocytic protoporphyrin concentration correlates with iron availability. *Blood Cells Mol Dis* 54:71–77.

30. Lyoumi S, et al. (2007) Increased plasma transferrin, altered body iron distribution, and microcytic hypochromic anemia in ferrochelatase-deficient mice. *Blood* 109:811–818.

31. Delaby C, et al. (2009) Excessive erythrocyte PPIX influences the hematologic status and iron metabolism in patients with dominant erythropoietic protoporphyria. *Cell Mol Biol* 55:45–52.

32. Egan DN, Yang Z, Phillips J, Abkowitz JL (2015) Inducing iron deficiency improves erythropoiesis and photosensitivity in congenital erythropoietic porphyria. *Blood* 126:257–261.

33. Deacon AC, Elder GH (2001) ACP Best Practice No 165: Front line tests for the investigation of suspected porphyria. *J Clin Pathol* 54:500–507.

34. Lockwood WH, Poulos V, Rossi E, Curnow DH (1985) Rapid procedure for fecal porphyrin assay. *Clin Chem* 31:1163–1167.

35. Lim CK, Li FM, Peters TJ (1988) High-performance liquid chromatography of porphyrins. *J Chromatogr A* 429:123–153.

36. Yien YY, et al. (2014) TMEM14C is required for erythroid mitochondrial heme metabolism. *J Clin Invest* 124:4294–4304.

37. Chen C, et al. (2013) Snx3 regulates recycling of the transferrin receptor and iron assimilation. *Cell Metab* 17:343–352.

38. Glynn SE, Martin A, Nager AR, Baker TA, Sauer RT (2009) Structures of asymmetric ClpX hexamers reveal nucleotide-dependent motions in a AAA+ protein-unfolding machine. *Cell* 139:744–756.